Indian Journal of Pure & Applied Physics
Vol. 62, September 2024, pp. 779-788
DOI: 10.56042/ijpap.v62i9.11354

Study of Co and Mn-doped ZnO Thin Films Electrodeposited on Aluminum Substrate: Comparison of Structural, Morphological and Hydrophobic Properties

Zehira Belamri* & Nehla Mermoul

Phase Transformation Laboratory, Frères Mentouri_Constantine 1University, Constantine, 25000 Algeria

Received 24 May 2024; accepted 1 August 2024

This work is the first study of the Mn and Co dopants effect on the physical properties of ZnO thin films electrodeposited on aluminum substrate.In order to synthesize these samples, electroplated Zn thin layers were thermally oxidized in atmospheric air for 2 h at 500 °C. The elaborated films were analyzedby X-ray diffraction (XRD), Raman spectroscopy, and scanning electron microscopy (FEG-SEM) equipped with energy dispersive X-ray analysis (EDX). The contact angle between the surface of the films and a deposited water drop (WCA) is measured to evaluate the wettability properties of the synthesized films.Mn and Co-doped ZnO thin films were studied and compared in order to better understand the effects of the dopant element on the physical properties of the host crystal, and to improve their hydrophobic properties.XRD analyses of a prepared mico/nanostructured material confirm the incorporation of substitutional transition metal ions on cation sites, and no secondary phase linked to Mnor Co is detected. This result was checked with EDX analysis. However, with increasing Mnor Co concentration, new modes appear in the Raman spectroscopy.The FEG-SEM images show that the surface morphologies change with dopant nature. The Mn-doped sample shows flower-like microstructures with an average size of 9µm, which are covered with spherical ZnO nanostructures with a size around 28 nm. This can lead to an improvement of the hydrophobicity of the ZnO coating compared to Co-doped films.

Keywords: ZnO thin films; Hydrophobicity; Thermal oxidation; Mn-doped ZnO; Co-dopedZnO; Mico/nanostructure

1 Introduction

Zinc oxide (ZnO) is a versatile semiconductor material with unique properties and wide-ranging applications, attracting significant research interest, with a direct wide bandgap of 3.37 eV and a large exciton binding energy of 60 meV at room temperature[1], ZnO offers excellent potential for optoelectronic devices, such as light-emitting diodes[2], laser diodes[3], and photodetector[4]. Additionally, ZnO has found applications in photocatalysis[5], gas sensing[6], and energy harvesting devices owing to its chemical and thermal stability, non-toxicity, and low cost. ZnO finds its role in the field of hydrophobicity[7-9], it has further uses on metallic surfaces; due to its strong self-cleaning features[10],and the low surface free energy of the (002) planes in the Wurtzite structure[11], resistance to adhesion to snow or ice[12], oil-water separation[13], and anti-corrosion[14], *etc*.[15–17].In our recent study, it's found that the hydrophobicity of the ZnO thin films can be improved by the dopingwith low amount of manganese (Mn)[18]or cobalt (Co)[19]. It is known that manganese (Mn) and cobalt (Co) have shown promising results in modifying the structural, optical[20], and magnetic[21,22] properties of ZnO. The similarity in ionic radius of Mn and Zn atoms leads to a higher solubility of Mn in the ZnO crystal lattice, and helps to improve the ZnO proprieties by tuning its size and band gap[23,24].The Mn-doped ZnO thin films show higher optical and electrical conductivity in UV region, and their band gap decreases with Mn doping[25].Recent results show that the decrease of the optical band gap energy from 3.24 eV to 3.05 eVlinked to the doping by Co in ZnO which gives rise to band gap bowing in studied thin films[26]. The same authors affirm that the M-H curve of ZnO:Co thin films confirms the good ferromagnetism in the studied sample[26].Co doped samples reveal good ferromagnetic properties, which is used in the field of optoelectronic and spintronics applications, and show good sensing behavior at room temperature due to the defects like oxygen vacancies[26]. In addition to ferromagnetism, Cobalt as a dopant in ZnO is advantageous for improving photocatalytic performance of ZnO because it reduces charge carrier recombination[27].

*Corresponding author:
(E-mail: belamri.zehira@umc.edu.dz)

In this context, the present study aims to investigate the effect of Mn and Co doping with different concentration on the structural, morphological, and especially the wetting properties of ZnO thin films deposited on aluminum substrates using a low-cost and simple electroplating technique. By employing a range of characterization techniques, including X-ray diffraction (XRD), Raman spectroscopy, scanning electron microscopy (SEM), and contact angle measurements, this work provides valuable insights into the influence of doping on the properties of ZnO thin films. Understanding the impact of Mn and Co doping on the hydrophobic characteristic of ZnO thin films on aluminum substrate is crucial for tailoring and optimizing these materials for specific applications. The findings of this study contribute to the growing body of knowledge in the field of doped ZnO materials and pave the way for the development of novel functional materials with improved properties for various technological applications.

2 Experimental

2.1 Substrate Preparation

Aluminum is chosen as substrate in this work due to its advantageous properties for various industrial applications. Before deposition, the substrates were mechanically polished with abrasive papers until the desired surface shape and thickness of 1 mm was obtained. The substrates were then cleaned ultrasonically in a sequence of methanol and distilled water baths, each for 15 minutes.

2.2 Materials

Zinc acetate dehydrate (Zn $(CH_3COO)_2$-$2H_2O$, 99%, Sigma-Aldrich, Germany) is taken as precursor for zinc. **C**obalt acetate (Co (CH_3COO), $4H_2O$, 98.5%, Lobachimie, India) and manganese acetate ($Mn(CH_3COO)_2$, 98%, Sigma-Aldrich, Germany) as the precursors for Co and Mn, respectively. Acetic acid (CH_3COOH) was used as the complexing agent and distilled water as solvent in order to prepare a clear solution.

2.3 Thin films preparation

A 0.2 M solution of zinc acetate dihydrate(Zn $(CH_3COO)_2$-$2H_2O$) precursor was prepared by dissolving it in 40 mL of distilled water. For doped films, appropriate amounts (0.1, 0.5, 2, 4, and 6 %) of cobalt acetate (Co (CH_3COO), $4H_2O$) or manganese acetate ($Mn(CH_3COO)_2$,) were added to the base solution. Undoped ZnO, Co-doped ZnO(CZnO), and Mn-doped ZnO(MZnO) thin films on the aluminum substrates were prepared using thermal oxidation of electroplated Zn layers. The electrochemical deposition was performed at -10 V for 15 minutes with an electrode separation distance of 1.5 cm. Following deposition of zinc metal, the films were subjected to thermal oxidation at 500 °C for 2 hours to obtain ZnO thin films.

2.4 Characterizations

PANALYTICAL empyrean diffractometer (XRD, Cu K_α radiation, λ = 1.540 Å, in the range from 10° to 80°) is used to examine the present phases and their orientations. XRD data were used to calculate the crystallites size using Scherrer formula, Eq. 1[28]:

$$D = \frac{K\lambda}{\beta cos\theta_B} \quad \ldots(1)$$

Where:

K: is a constant known as shape factor (k=0, 94)
λ: is the X-ray wavelength of 1.5406 Å
θ_B: is the Bragg diffraction angle
β:is the FWHM (full width at half maximum) of θ_B.

The specific values of the lattice parameters a and c were calculated using the established formulas for the hexagonal crystal structure, as detailed in the relevant literature, Eq. 2 &3[29,30].

$$a = \frac{\lambda}{\sqrt{3} * sin\theta} \quad \ldots(2)$$

$$c = \frac{\lambda}{sin\theta} \quad \ldots(3)$$

Where:
λ :is the wavelength of X-rays (0,1540nm)
θ: is diffraction angle of (100) a parameter and the peak (002)for c parameter.

The dislocation density (δ) and microstrain (ε) values provide insights into the defect states and strain within the doped ZnO thin films. These parameters are calculated from the XRD data using the Williamson-Smallman (Eq. 4) and Williamson-Hall equations (Eq. 5)[31].

$$\delta = \frac{1}{D^2} \quad \ldots(4)$$

$$\varepsilon = \frac{\beta cos\theta}{4} \quad \ldots(5)$$

The biaxial stress e_{zz} along the c axis perpendicular to the substrate plane is calculated from the lattice parameter c, Eq. 6[32]:

$$e_{zz}(\%) = \frac{c-c_0}{c_0} \times 100 \quad \ldots(6)$$

Where:
c :is the lattice parameter of the elaborated ZnO films,
c_0 : is the unstrained ZnO lattice parameter (0.5207 nm).
The residual stress σ parallel to the layer surface is expressed as[33]:

$$\sigma = \frac{2c_{13}^2 - c_{33}(c_{11}+c_{12})}{2c_{13}} \times \frac{c-c_0}{c_0} \quad \ldots(7)$$

Here Cij are the elastic stiffness constans for single crystal ZnO ($C11$ =208.8GPa, $C33$=213.8GPa, $C12$=119.7GPa ,13 = 114.2GPa).

$\sigma = -233 \times \varepsilon_z$ (8)

Raman spectra are recorded using HORIBA LabRAM HR Evolution type spectrometer at room temperature with a monochromatic radiation source of 473 nm. The morphological and elemental analyses are performed using a Field Emission Gun Scanning Electron Microscope (SEM, Jeol FEG JSM-7100 F) equipped with energy dispersive X-ray spectrometer (EDX). The contact angle measurements are carried out 5 seconds after the deposit of a water drop with a volume of 5 µL on the elaborated thin films using a LEYBOLD type light source (6 V, 30 W) and a projection lens, which allows the static image of the drop displayed on a 30×30 cm^2 screen to be enlarged.

3. Results and discussions

3.1 Structural properties

X-ray diffraction (XRD) patterns have provided valuable insights into the structural properties and crystalline nature of undoped and doped ZnO thin films. (Figs. 1 (a) and 1(b)) show the diffraction patterns obtained of elaborated samples. The XRD patterns revealed that the undoped, Mn-doped, and Co-doped ZnO thin films exhibited a polycrystalline wurtzite structure, with diffraction peaks corresponding to the (100), (002), (101), (102), (110), (103), (112), (201), and (202) planes (referred to ICDD No. 01-070-2551). The predominant peak located around 36.298° corresponds to the (101) plane, indicating preferential orientation along this

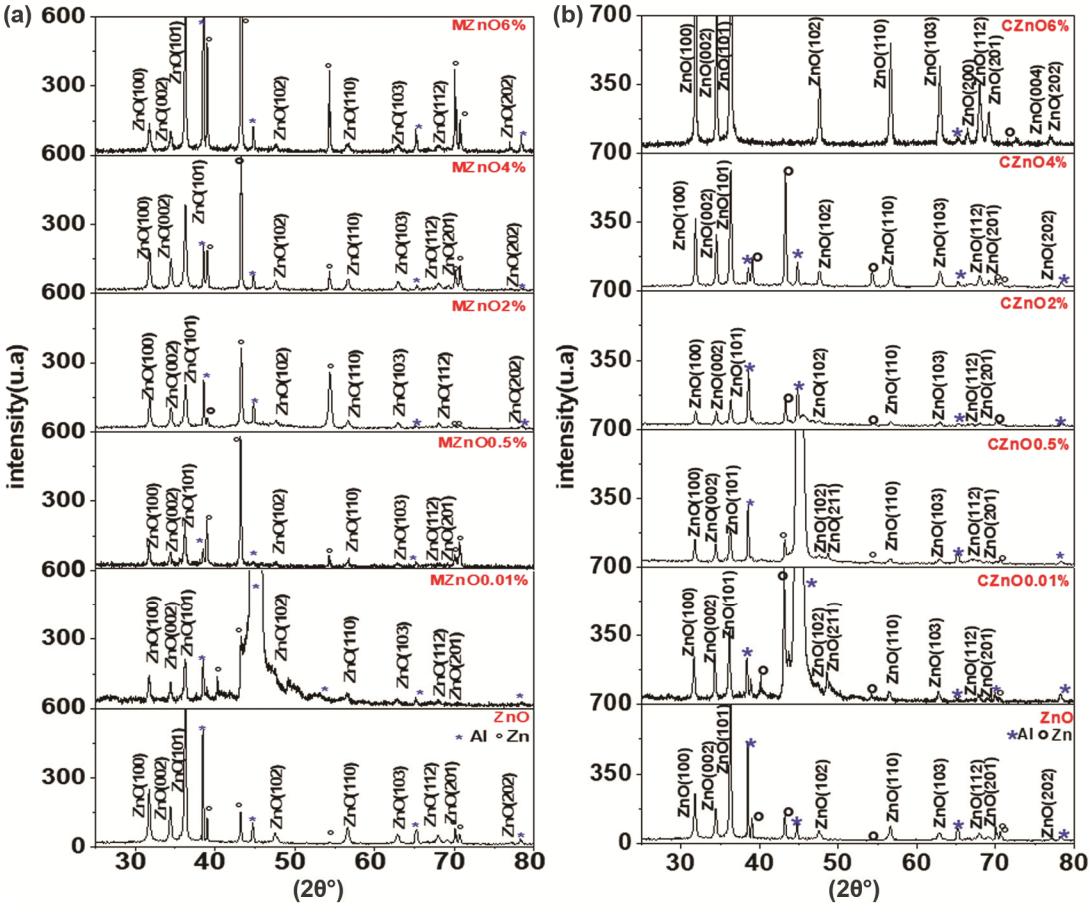

Fig. 1 — XRD patterns of (a) Mn-doped ZnO and (b) Co-doped ZnO thin films

direction of the deposited films. No peaks from Mn or Co oxides were observed, confirming successful substitution of dopant element.

3.1.1 Crystallites Size

The (101) peak intensity decreased with increasing Mn or Co doping concentration (≤ 4% Mn), then increased at 6% doping concentration. The decrease in (101) peaks intensity wen the concentration increase can be explained by crystallites size. At lower Mn or Co concentrations (≤ 4%) , the decrease in crystallites size due to strain caused by incorporation of manganese ions into zinc ion sites (Table 1) accompanying decreased of diffraction peaks intensity more than that of pure films this effect is also observed in other previous studies[31]. But it can be seen that at 6% concentration the opposite occurred. This variation in peak intensity shows the effect of doping concentration on surface texture of the films.

3.1.2 Lattice Parameters and Strain

Both Mn and Co doping lead to minor variations in the individual lattice parameters a and c, and the values of FWHM changed compared to undoped ZnO. These observed variations can be attributed to the intricate interplay between two competing effects: the lattice contraction resulting from the substitution of the smaller dopant ions (Mn^{2+}or Co^{2+}) into the Zn^{2+} sites, and the lattice expansion arising from the insertion of the dopant atoms within the ZnO crystal structure.

For Mn-doped ZnO (MZnO) films, the c/a ratio remains very close to the ideal hexagonal value of 1.60 for ZnO, even at different Mn concentrations (values ranging from 1.601 to 1.602 in Table 1). This indicates that the wurtzite structure of ZnO is largely preserved with Mn doping. In contrast, for Co-doped ZnO (CZnO) films, the c/a ratio deviates significantly from the ideal value of 1.60, remaining constant at 1.732 in the (Table 1) for all Co concentrations. This constant deviation suggests a distortion of the wurtzite structure in the Co-doped films.

The observed preservation of the wurtzite structure in MZnO films and its distortion in CZnO films can be attributed to the difference in ionic size mismatch between the dopants and Zn^{2+}. The smaller mismatch between Mn^{2+} (0.067 nm) and Zn^{2+} (0.074 nm) allows for better accommodation of Mn ions within the ZnO lattice, maintaining the overall crystal structure. However, the larger mismatch between Co^{2+} (0.058 nm) and Zn^{2+} leads to a more significant distortion of the wurtzite structure in the CZnO films.

3.1.3 Dislocation Density and Microstrain

The dislocation density (δ) and microstrain (ε) values provide insights into the defect states and strain within the doped ZnO thin films. For both Mn-doped ZnO (MZnO) and Co-doped ZnO (CZnO) films, the dislocation density and microstrain values increase at lower doping concentrations (up to 4%) compared with pure sample (Table 2).This increase is attributed to the decrease in crystallites size (D) associated with an increase in grain boundaries caused by the incorporation of dopant ions (Mn^{2+}orCo^{2+}) into the ZnO lattice[31]. However, at the highest doping concentration (6 % Mn or 6 % Co), the dislocation density and microstrain values decrease for both films; MZnO (0.444 x 10^{15}ligne/$m^2$and 0.7629 x10^{-3}, respectively) and CZnO (0.694 x 10^{15} lines/m^2 and 3.8142 x 10^{-3}, respectively). In order to stabilize the crystal structure, the size of the crystals is decreased to release the internal strain[34].

3.1.4 Biaxial Stress and Residual Stress

The stress state in the prepared layers can be determined using XRD spectra. The biaxial stress e_z along the c axis perpendicular to the substrate plane is

Table 1 — Lattice parameters and crystallites size of undoped, Mn-doped and Co-doped ZnO thin

Samples	$2\theta_{101}$(°)	FWHM(°)	D(nm)	c_0	c(Å)	a(Å)	c/a
UndopedZnO	36,299	0,225	39	5,207	5,2062	3,2501	1,602
MZnO 0.01%	36,263	0,315	28	5,207	5,2055	3,2507	1,601
MZnO0.5%	36,240	0,257	34	5,207	5,2069	3,2504	1,602
MZnO2%	36,319	0,324	27	5,207	5,1955	3,2440	1,602
MZnO4%	36,278	0,297	29	5,207	5,1973	3,2450	1,602
MZnO6%	36,280	0,184	47	5,207	5,1987	3,2472	1,601
CZnO0.01%	36,142	0,281	31	5,207	5,2226	3,0153	1,732
CZnO0.5%	36,250	0,301	29	5,207	5,2053	3,0053	1,732
CZnO2%	36,324	0,284	31	5,207	5,1974	3,0072	1,732
CZnO4%	36,321	0,264	33	5,207	5,1952	2,9995	1,732
CZnO6%	36,327	0,23	38	5,207	5,1938	2,9986	1,732

Table 2 — Dislocation density, microstrain, and Stress values of ZnO thin films

Samples	2θ101 (°)	FWHT (°)	D (nm)	Dislocation density δx 10^{15} (ligne/m^2)	Lattice Deformation (εx10^{-3})	e_{zz}%	σ(GPa)
UndopedZnO	36,299	0,225	39	0,664	0,9329	-0,04004	0,09329
0.01%Mn	36,263	0,315	28	1,302	1,3062	-0,07596	0,17699
0.5%Mn	36,240	0,257	34	0,866	1,0658	-0,00557	0,01297
2%Mn	36,319	0,324	27	1,377	1,3433	-0,55227	1,28680
4% Mn	36,278	0,297	29	1,157	1,2315	-0,48653	1,13362
6%Mn	36,280	0,184	47	0,444	0,7629	-0,41345	0,96333
0.01%Co	36,142	0,281	31	1,037	4,6625	0,78395	-1,82662
0.5%Co	36,250	0,301	29	1,189	4,9928	-0,08402	0,19578
2%Co	36,324	0,284	31	1,058	4,7098	-0,47922	1,11660
4%Co	36,321	0,264	33	0,914	4,3781	-0,58878	1,37186
6%Co	36,327	0,230	38	0,694	3,8142	-0,66176	1,54191

calculated from the lattice parameter c[29]. It is worth noting that the Co-doped ZnO films exhibit higher microstrain values compared to the Mn-doped films at all doping concentrations, suggesting a greater degree of lattice distortion in the CZnO films. This observation is consistent with the analysis of the c/a ratio, which showed a deviation from the ideal value for CZnO films, indicating a distortion of the wurtzite structure.

The biaxial stress (e_{zz}) along the c-axis and the residual stress (σ) parallel to the layer surface are interrelated. They exhibit opposite directions in the interface plane between the layer and the substrate. This highlights the importance of measuring the lattice parameter c, as it allows determining the stress state in different directions within the thermally oxidized layer. The strain can be either positive (tensile) or negative (compressive).

Table 2 presents the stress values for ZnO films doped with manganese and cobalt at various concentrations. A negative value of e_{zz} indicates compressive stress along the c-axis, accompanied by positive values of residual stress σ. This positive σ suggests that the films experience an attractive force parallel to the substrate surface. The stress in the films arises from impurities (doping elements), defects (reduction in vacancies), and lattice distortions (grain growth) within the crystal structure. However, for the 0.01% Co concentration, the positive value of e_{zz} corresponds to tensile stress.

A comparison of the obtained results reveals that the thermally oxidized Mn-doped ZnO thin films exhibit preferential growth along the (101) axis, a low dislocation density, and minimal deformation. This indicates that these films are of higher quality compared to the Co-doped ZnO thin films.

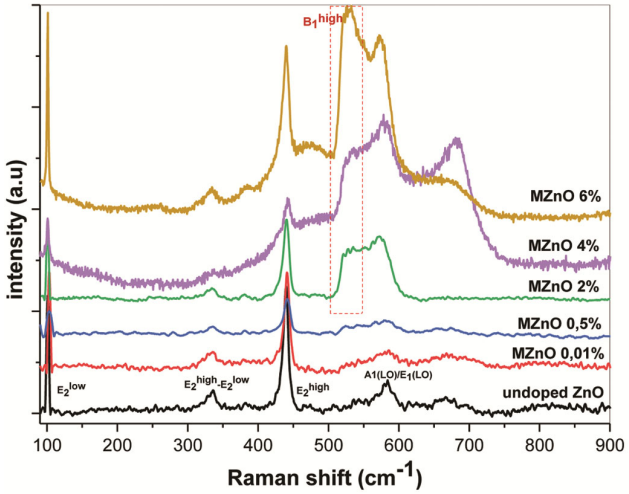

Fig. 2 — Raman spectra of undoped and Mn-doped ZnO thin films

Raman spectroscopy is highly sensitive for detecting crystallinity, structural disorders, and defects in micro and nanostructures. In this work, the vibration properties of Co and Mn-doped ZnO thin films were investigated using Raman scattering technique. The Raman spectra of undopedZnO thin films and those doped with Mn (0.01%, 0.5%, 2%, 4%, and 6%) after annealing at 500°C for 2h are presented in (Fig. 2). For 0.01% and 0.5% Mn concentrations, five peaks corresponding to $E_2^{(low)}$, $E_2^{(high)}$-$E_2^{(low)}$, A_1(TO), $E_2^{(high)}$ and A_1(LO)/E_1(LO) modes of hexagonal ZnO phonons were observed, compared to the purchased ZnO powder reference (Fig. 3).

The high intensity of the $E_2^{(high)}$ peak, arising from vibrations of the oxygen sublattice in the ZnO crystal[35,36], reflects the good crystallization quality of the hexagonal wurtziteZnO thin films[37]. This corroborates the XRD results. The shifts of this peak to lower or higher wavenumbers are attributed to

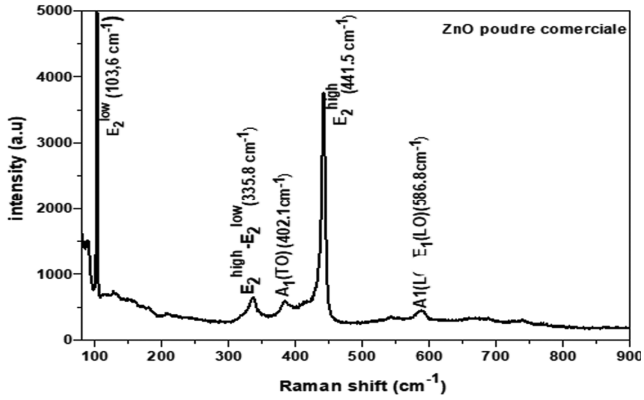

Fig. 3 — Raman spectra of purchased ZnO powder as reference (Purchased from Fluka Analytical Company)

changes in chemical bonds and atomic symmetry[38]. Hence, variations in chemical bond lengths due to Mn doping into the ZnO lattice lead to wavenumber shifts. Moreover, the $E_2^{(high)}$ peak position is highly sensitive to the intrinsic residual stress[39,40]. The calculated residual stress values show the Mn-doped ZnO films experience an attractive force ($\sigma>0$) parallel to the substrate, so the $E_2^{(high)}$ peak shifts to higher wavenumbers with increasing Mn content.

At high Mn doping levels (2%, 4%, 6%), the main undopedZnO peaks are still visible, although the overall Raman spectrum shape changes, indicating slight degradation of structural quality. A new vibration mode called the $B_1^{(high)}$ silent mode appears between 500-740 cm^{-1} near the $A_1(LO)/E_1(LO)$ modes of hexagonal ZnO[41,42].

Figure4 shows the Raman spectra of Co-doped ZnO compared to undoped ZnO and Co_3O_4 thin films (Fig. 5). Two main effects are evident with increasing Co doping: first, the ZnO phonon modes weaken and broaden considerably with higher Co content. However, the $E_2^{(high)}$ mode is still retained for 6% Co, albeit with low intensity. This peak shifts to higher wavenumbers with increasing Co concentration due to residual stress effects in Co-doped ZnO films. The broadening of phonon modes reflects deterioration of the host ZnO lattice caused by distortions in the local atomic arrangement around impurities (attributed to Co incorporation into the ZnO lattice). Additional sharp Raman bands appear at 493 cm^{-1}, 532 cm^{-1} and 719 cm^{-1} for the 6% Co-doped sample, accompanying the weakening of ZnO host phonon modes. These new sharp peaks resemble the E_g, F_{2g}, and A_{1g} phonon modes of Co_3O_4[42].

The Raman spectrum indicates there is grain segregation of the Co_3O_4 phase in the 6% Co-doped

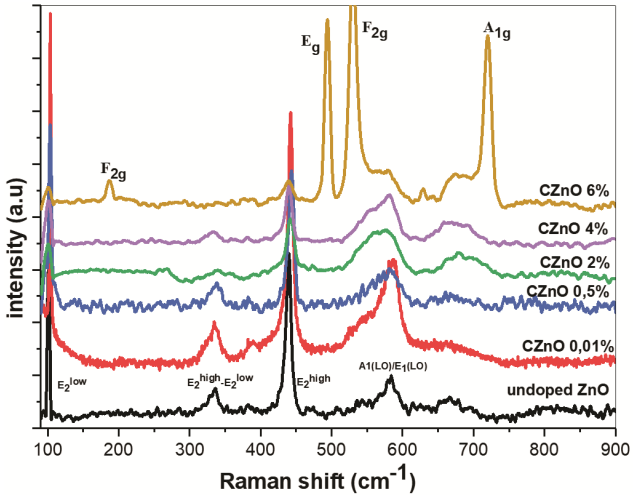

Fig. 4 — Raman spectra of undoped and Co doped ZnO thin films

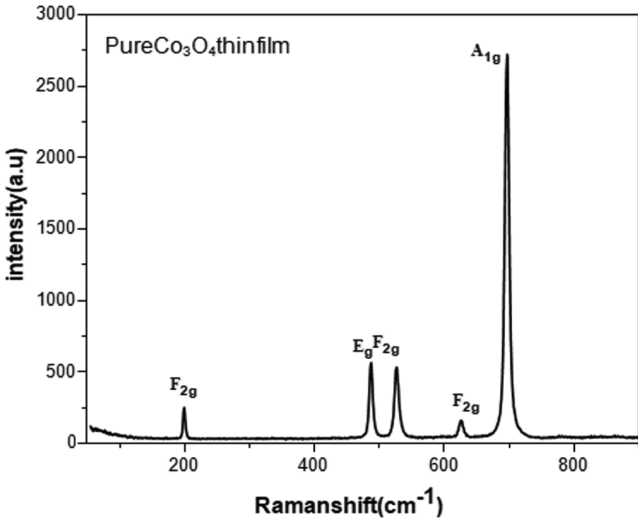

Fig. 5 — Raman spectra of pure Co_3O_4 thin film prepared as reference

ZnO thin film. Comparison with the pure Co_3O_4 thin film spectrum (Fig. 5) shows the E_g, F_{2g}, and A_{1g} phonon modes of the doped film shift up to 10 cm^{-1} higher, which can be explained by stresses experienced by the Co-doped ZnO grains. Based on these Raman results, the absence of secondary phases related to Mn or Co in the XRD spectra can be attributed to their low concentrations being undetectable by XRD, as the diffraction peaks may not be strong enough to distinguish from the background. Thus, from the XRD and Raman data, it can be deduced that while Co incorporation into ZnO decreases the crystal quality of the ZnO thin layer, there is no change in the wurtzite crystal structure at low Co doping concentrations.

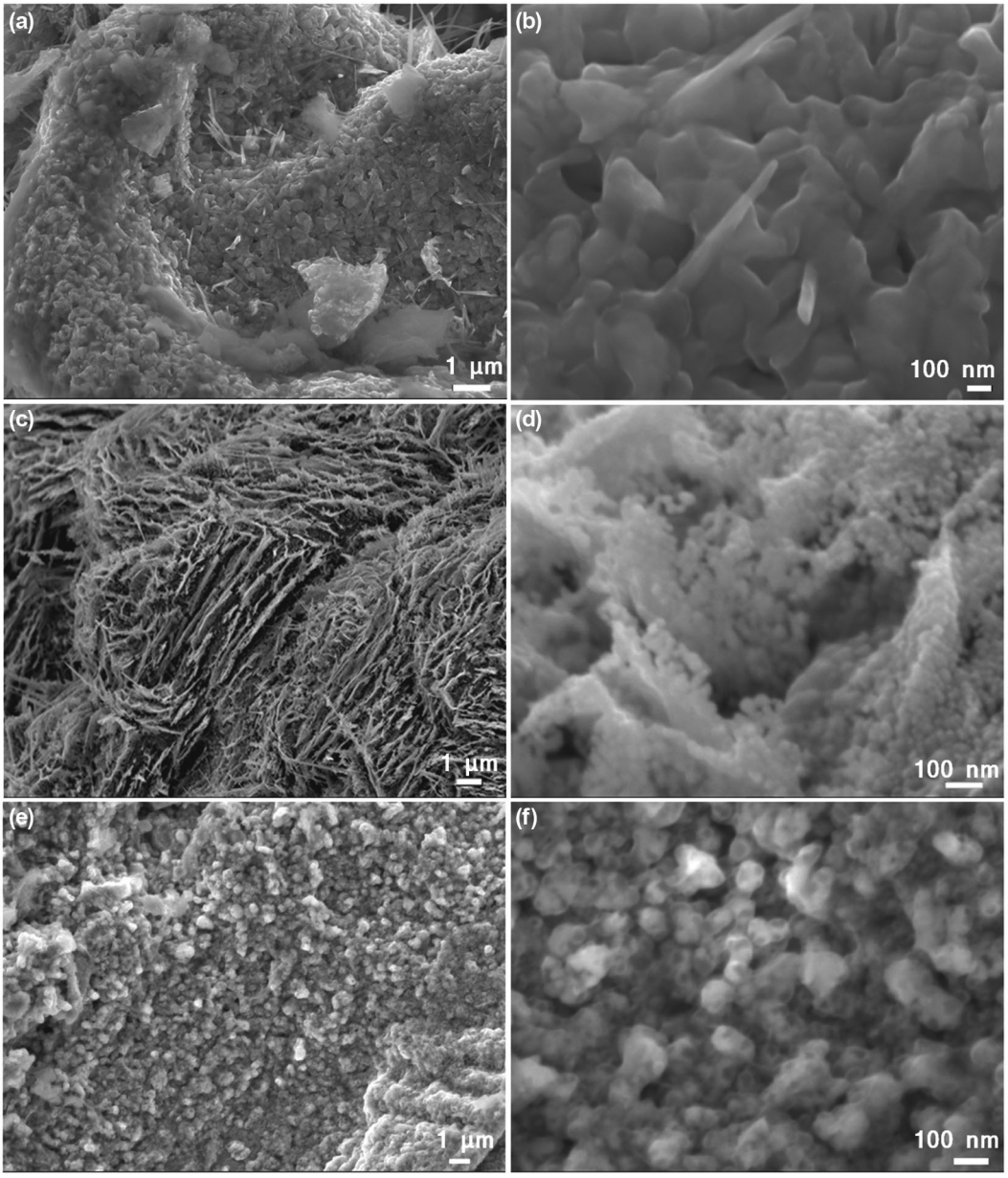

Fig. 6 — FEG-SEM images of (a) undoped ZnO thin film, (b) 0,01% Mn-doped ZnO, (c) 0,01% Co-doped ZnO. Right column (image (d), (e) and (f)) are the larger magnification images of the same films.

3.2 Morphological properties

The surface morphologies of the undoped, Mn-doped ZnO, and Co-doped ZnO thin films deposited on the aluminum substrates were investigated using Field Emission Scanning Electron Microscopy (Fig. 6(a-f)) & Fig. 7 (a-c) are the corresponding Energy Dispersive X-ray Spectroscopy (EDS) patterns.

As shown in Fig. 6 (a), the undoped ZnO film exhibits a compact morphology, however, the surface morphology changed upon the introduction of Mn or Co dopants. FEG-SEM images of the 0.01% Mn-doped ZnO thin film (Fig. 6(b)) reveal the formation of slightly deformed, flower-shaped structures with a conical or pyramidal shape. These deformed flowers are covered with a large number of spherical ZnO nanostructures (Fig. 6 (e)), which roughen the surface of the elaborated thin layers.

In contrast, the FEG-SEM images of the Co-doped ZnO thin films (Fig. 6(c)) shows a more uniform and compact morphology with homogeneously dispersed ZnO nanostructure.EDXanalysis (Fig. 7(a-c)) confirms the presence of zinc and oxygen in the

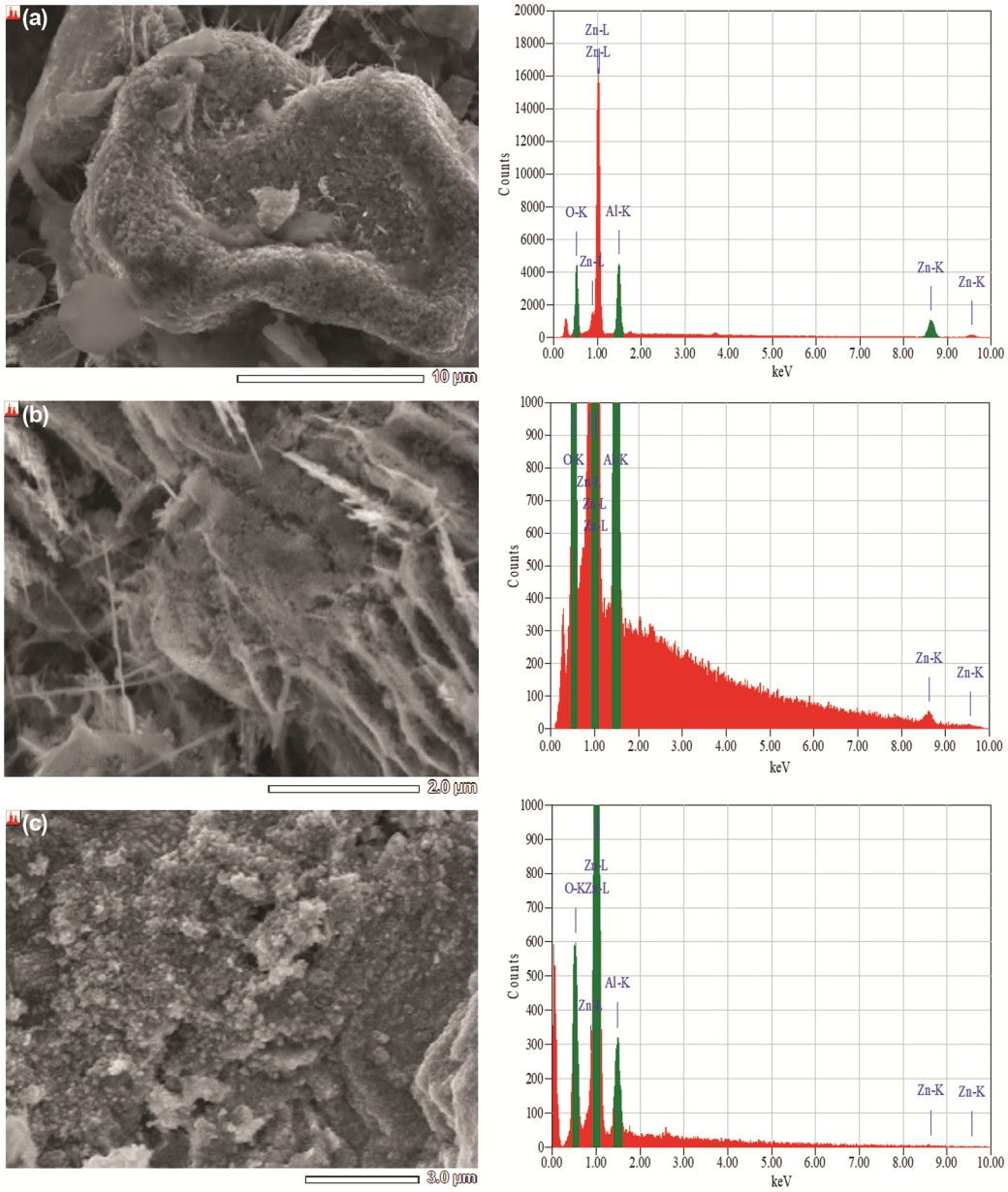

Fig. 7 — EDS analysis of (a) undoped ZnO thin film, (b) 0,01% Mn-doped ZnO, (c) 0,01%Co-doped ZnO with suitable indexing.

ZnO thin films, but no Mn or Co elements were detected along with zinc and oxygen in the doped samples, which can be attributed to their low doping concentrations.

3.3 Hydrophobic properties

The wetting properties of the thermally oxidized undoped ZnO layer and Mn-doped ZnO layers on the Al substrate were analyzed by measuring the water contact angle of these films, as shown in Fig. 8 (a-f) and Fig. 9 (a-f). The measurements reveal that the undoped ZnO film exhibits an inherently hydrophobic nature, with a contact angle of 120.91° (Fig. 8 (a)). The droplet shape on the surface of the undoped ZnO film was highly specific, indicating the hydrophobic character of this structure. The increase in water contact angle observed for the Mn-doped ZnO coatings can be attributed to their morphological features. The samples doped with low Mn concentrations (0.01% and 0.5%) exhibited deformed flower-like structures covered with spherical ZnO nanostructures (Fig. 6 (b)). This surface roughness traps air on the substrate, preventing water from adhering to the ZnO film and leading to the

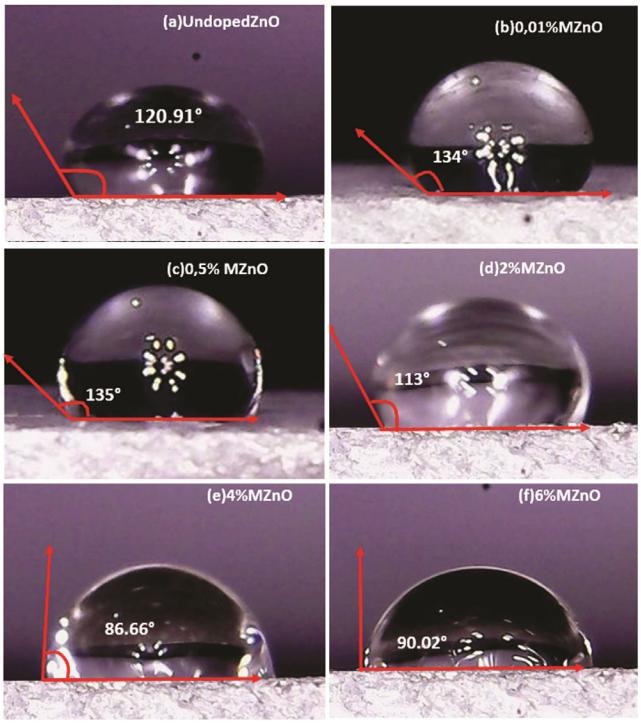

Fig. 8 — Contact angle of (a) undoped ZnO and Mn-doped ZnO thin films (Mn concentrations are indicated on pictures)

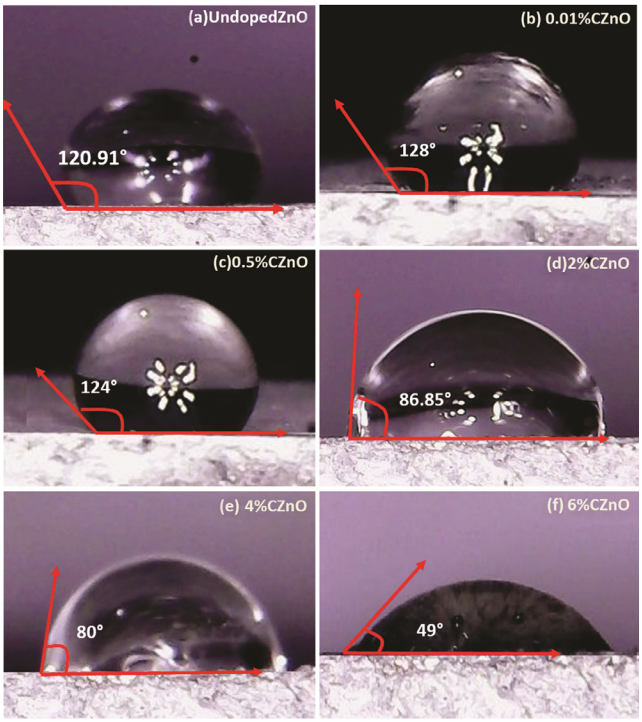

Fig. 9 — Water contact angle of (a) pure ZnO and Co doped ZnO thin films (Co concentrations are indicated on pictures)

hydrophobicity of these coatings.However, as the Mn doping concentration is increased, the contact angle decreases, and the surface becomes hydrophilic at Mn concentrations of 4% (Fig. 8(e)) and above. A similar trend is observed for the Co-doped ZnO thin films, where the surface transitions from hydrophobic to hydrophilic at Co concentrations from 2% to 6% (Fig. 9(a-e)). This change in wettability may be associated with the reduced surface roughness and increased porosity in the ZnO film structure at higher dopant concentrations.

4 Conclusion

The main objective of this work was to prepare and characterize undoped and doped ZnO thin films deposited on aluminum substrates, with a focus on understanding the influence of doping on the physical properties and hydrophobic behavior of the elaborated thin films.

The structural analysis by XRD confirm the formation of a hexagonal Wurtzite ZnO nanostructure structure in the all pepared thin films, regardless of the dopant type and concentration. The decrease in peak intensity and shift in the preferred orientation (101) peak position were attributed to the incorporation of the dopant ions into the ZnO lattice, leading to changes in the crystallite size and internal stresses. Raman spectroscopy provided further insights into the structural quality of the films. For low Mn doping concentrations, the characteristic of ZnO phonon modes were retained, indicating minimal degradation of the crystal structure. However, at higher Mn and Co concentrations, the broadening and weakening of the ZnO modes, along with the emergence of new peaks, suggested increased structural disorder due to the incorporation of the dopants.

The surface morphology of the preperd films, observed by scanning electron microscopy, showed a strong correlation with the hydrophobic properties. The formation of deformed flower-like structures covered with spherical ZnO nanoparticles at low Mn doping concentrations resulted in trapping of air pockets on the surface, leading to enhanced hydrophobicity. Increasing the dopant concentration, on the other hand, led to a more uniform and compact surface morphology, reducing the hydrophobic character of the films.Overall, the results indicate that the incorporation of low concentrations (0.01% and 0.5%) of Mn into the ZnO lattice is more effective in improving the structural quality and hydrophobic behavior of the studied thin films compared to Co doping under the same deposition conditions. These findings provide valuable insights into the design and

development of hydrophobic coatings with tailored properties using ZnO-based materials.

Conflict of Interest Statement

The authors declare that they have no known competing financial interests or personal relationships that could have appeared to influence the work reported in this paper.

References

1 Truong V D T, Nguyen T TT, Vo T L, Huynh H T & Pham T K H, *J Tech Educ*, 72 (2022) 39.
2 Zhou R, Ying Wu X, Zhao Q, Kai Liu K, Dong L & Xin S C, *J Lumin*, 252 (2022) 119425.
3 Lan Y, Yang G, Zhao Y, Liu Y & Demir A, Appl Surf Sci, 596 (2022)153506.
4 Nurfani E, Nulhakim L, Muhammad D M, Rozana M & Astuti W, *Opt Mater*, 148 (2024) 114948.
5 Al-Rasheedi A, Salwati A, Ansari A R, Hassaneen A A D & Aida M S, *Inorg Chim Commun*, 158 (2023) 111568.
6 Kang Y, Yu F, Zhang L, Wang W, Chen L & Li Y, *Solid State Ionics*, 360 (2021) 115544.
7 Belamri Z, Boumaza L & Boudjadar S, *Phys Scr*, 98 (2023) 125949.
8 Belamri Z, Darenfad W & Guermat N, *Eur Phys J Appl Phys*, 99 (2024) 10.
9 Belamri Z, Darenfad W & Guermat N, *J Nano-Electron Phys*, 15 (2023).
10 Nundy S, Ghosh A & Mallick T K, *ACS Omega*, 5 (2020) 1033.
11 Abdulrahman A F, Barzinjy A A, Hamad S M & Munirah A A, *ACS Omega*, 47 (2021) 31595.
12 Liu G Y, Yuan Y, Liao R J, Xiang H Y, Wang L, Yu Q & Zhang C, *Surf Interfaces*, 28: (2022) 101588.
13 Zhang X, Mo Z, Arenal R, Li W & Wang C, *Appl Surf Sci*, 609 (2023) 155208.
14 Zhu M, Yuan R, Wang C, Gao Q, Wang H & Qian H, *Appl Surf Sci*, 615 (2023) 156287.
15 Sotoudeh F, Mousavi S M, Karimi N, Lee B J, Abolfazli-Esfahani J & Manshadi M K D, *Alex Eng J*, 68 (2023) 587.
16 Zhao J, Gao X, Chen S, Lin H, Li Z & Lin X, *Compos Part B-Eng*, 243 (2022) 110104.
17 Muñóz A J, Reca J & Martínez J, *Sci Rep*, 14 (2024) 8236.
18 Belamri Z, Mermoul N & Hamana D, *Acta* Phys Pol A, 145 (2024) 301.
19 Belamri Z, *Springer Proc Mater*, 45 (2023) 125.
20 Saqib M, Rahman S, Ali S, Khan S A, Ismail B & Khan A M, *Mater Today Commun*, 37 (2023) 107335.
21 Naziba A T, Nafisa M T, Sultana R, Ehsan M F, Tareq A R M, Rashid R, Das H , AtiqueUllah A K M & Fazle K A K M, *J Magn Magn Mater*, 171836 (2024).
22 Narasimman S, Balakrishnan L & Alex Z C, *Mater Sci Semicond Process*, 166 (2023) 107732.
23 Dhivya A, Yadav R & Packiam S, *Mater Today Proc*, 48 (2022) 494.
24 Darenfad W, Guermat N & Mirouh K, *J Mol Struct*, 1286 (2023) 135574.
25 Güneri E, Henry J, Göde F & Özpozan N K, *J Cent South Univ*, 30 (2023) 691.
26 Abirami N, A M S Arulanantham & K S Joseph Wilson, *Mater Res Express*, 7 (2020) 02640.
27 Marinov G, Georgieva B, Vasileva M & Babeva T, *Appl Sci*, 13 (2023) 9611.
28 Manh D H, Nha T T N, Phon L T H, Nam P H, Than T D & Phong P T, *RSC Adv*, 13 (2023) 25007.
29 Zhao J, Ni J, Zhao X & Xiong Y, *J Wuhan Univ Technol-Mater Sci Ed*, 26 (2011) 388.
30 Li X, Zhu X & Jin K, *Opt Mater,* 100 (2020) 109657.
31 Balamurali S, Saravanakumar S, Chandramohan R & Magudeswaran P N, *Braz J Phys*, 51 (2021) 1501.
32 Rao T P, Kumar M S, Angayarkanni S A & Ashok M, *J Alloys and Compd*, 485 (2009) 413.
33 Ong C B, Ng L Y & Mohammad A W, Renew Sustain Energy Rev, 81 (2018) 536.
34 Singh B, Shrivastava S B & Ganesan V, *J Nanoscience* 16 (2017) 1650024.
35 Dasi G, Lavanya T, Suneetha S, Vijayakumar S, Shim J-J & Thangaraju K, *Spectrochimica Acta Part A: Mol Biomol Spectrosc*, Elsevier Science, 265 (2022) 120377.
36 Kasirajan K, Chandrasekar L-B, Maheswari S, Karunakaran M & Sundaram P S, *Opt Mater*, 121 (2021) 111554.
37 Thiruvengadathan R, Dhua S, Rani S, Mathai C-J, Bai M, Gangopadhyay K & Gangopadhyay S, *Mater Adv*, 3 (2022) 5383.
38 Raskar N D, Dake D V, Mane V A, Stathatos E, Deshpande U & Dole B, *J Mater Sci Mater Electron*, 30 (2019) 10886.
39 Manjón F J, Mari B, Serrano J & Romero A H, *J Appl Phys*, 97 (2005) 053516.
40 Fenwick W E, Kane M H, Varatharajan R, Zaidi T, Fang Z, Nemeth B, Keeble D J , El-Mkami H, Smith G M,Nause J, Summers C J & Ferguson I T, *Zinc Oxide Mater Dev*, 6474 (2007) 273.
41 Zhou H, Chen L, Malik V, Knies C, M.Hofmann D, Bhatti K P & Chaudhary S, Klar P J, Heimbrodt W, Klingshirn C, Kalt H, *Phys Status Solidi (a)*, 204 (2007) 112.
42 Diallo A, Doyle T B, Mothudi B M, Manikandan E, RajendranV & Maaza M, *J Magn Magn Mater*, 424 (2017) 251.